# Velocity of change in vegetation productivity over northern high latitudes

Mengtian Huang, Shilong Piao, Ivan Janssens, Zaichun Zhu, Tao Wang, Donghai Wu, Philippe Ciais, Ranga Myneni, Marc Peaucelle, Shushi Peng, et al.

▶ **To cite this version:**

Mengtian Huang, Shilong Piao, Ivan Janssens, Zaichun Zhu, Tao Wang, et al.. Velocity of change in vegetation productivity over northern high latitudes. Nature Ecology & Evolution, 2017, 1 (11), pp.1649-1654. 10.1038/s41559-017-0328-y . hal-02894758

**HAL Id: hal-02894758**
**https://hal.science/hal-02894758**

Submitted on 7 Jun 2023

**HAL** is a multi-disciplinary open access archive for the deposit and dissemination of scientific research documents, whether they are published or not. The documents may come from teaching and research institutions in France or abroad, or from public or private research centers.

L'archive ouverte pluridisciplinaire **HAL**, est destinée au dépôt et à la diffusion de documents scientifiques de niveau recherche, publiés ou non, émanant des établissements d'enseignement et de recherche français ou étrangers, des laboratoires publics ou privés.

This is the accepted version of Huang, M., et al. “Velocity of change in vegetation productivity over northern high latitudes” in Nature ecology and evolution, vol. 1 (Nov. 2017), p. 2397-334X. DOI 10.1038/s41559-017-0328-y. This version is available at https://ddd.uab.cat/record/181846 under the terms of the All rights reserved license.

# Velocity of change in vegetation productivity over northern high latitudes

Mengtian Huang[1], Shilong Piao[1,2], Ivan A. Janssens[3], Zaichun Zhu[1], Tao Wang[2], Donghai Wu[1], Philippe Ciais[1,4], Ranga B. Myneni[5], Marc Peaucelle[4,6,7], Shushi Peng[1], Hui Yang[1], Josep Peñuelas[6,7]

[1] Sino-French Institute for Earth System Science, College of Urban and Environmental Sciences, Peking University, Beijing 100871, China.

[2] Institute of Tibetan Plateau Research, Chinese Academy of Sciences, Beijing 100085, China.

[3] Centre of Excellence PLECO (Plant and Vegetation Ecology), Department of Biology, University of Antwerp, Universiteitsplein 1, B-2610 Wilrijk, Belgium.

[4] Laboratoire des Sciences du Climat et de l’Environnement, CEA CNRS UVSQ, Gif-sur-Yvette 91190, France.

[5] Department of Earth and Environment, Boston University, Boston, Massachusetts 02215, USA.

[6] CREAF, Cerdanyola del Vallès, Barcelona 08193, Catalonia, Spain.

[7] CSIC, Global Ecology Unit CREAF-CSIC-UAB, Bellaterra, Barcelona 08193, Catalonia, Spain.

Manuscript for ***Nature Ecology & Evolution***

**Warming is projected to increase the productivity of northern ecosystems[1-3]. However, knowledge on whether the displacement of vegetation productivity isolines matches the northward motion of temperature isolines is still limited. Here, for the first time, we compared changes in the spatial patterns of vegetation productivity and temperature using the concept of velocity of change, which is defined as the ratio of temporal changes in a variable to the spatial gradient of the same variable, making it possible to express these two variables in the same unit of displacement per time[4-9] (e.g. km yr$^{-1}$). Normalized Difference Vegetation Index (NDVI) data from 1982 to 2011 was used to calculate the velocity of vegetation productivity north of 50°N. Our results show that the average velocity for growing season (GS) NDVI ($NDVI_{GS}$; 2.8±1.1 km yr$^{-1}$) is lower than that for GS mean temperature ($T_{GS}$; 5.4±1.0 km yr$^{-1}$). About 20% of the study area display larger velocities of $NDVI_{GS}$ than $T_{GS}$, mainly in eastern Europe, northeastern and southern Siberia, and parts of western Canada. By comparison, in northern Europe, western and central Siberia, and northeastern Canada (52% of the study area), the $NDVI_{GS}$ velocity is less than half of $T_{GS}$ velocity, indicating that the northward motion of productivity isolines is much slower than that of temperature isolines over the last 30 years. We tentatively attribute this mismatch between the velocities of vegetation productivity and temperature to the effects of limited resource availability and vegetation acclimation mechanisms. Analyses of the velocity of ecosystem productivity from ecosystem model simulations further suggested that limited nitrogen availability is a crucial obstacle for vegetation to track the warming trend.**

The Earth's climatic system is experiencing significant warming, which has raised concerns about the impacts on terrestrial ecosystems[10]. In-situ observations, manipulative experiments, as well as satellite-derived data have all pointed out that vegetation productivity is sensitive to temperature change in northern high latitudes[1,11-14].

Vegetation can adjust to climate change through relatively fast mechanisms (e.g. adjustment of phenology or physiology[15,16]) and through slower mechanisms (e.g. phenotypic and genotypic adaptations, changes in community composition[16]). If climate changes slowly and vegetation has ample time to adjust, it can be expected that warming would result in a northward shift of vegetation structure and function in the northern hemisphere. In reality, temperature acclimation and adaptation of plants[17], as well as limited resource availability such as nitrogen[18], may prevent vegetation productivity change from keeping the same rate as the rapid climate warming. To the contrary, $CO_2$ fertilization effects and regional nitrogen deposition may amplify the greening trend induced by warming temperature[3,19]. Unfortunately, knowledge about the rate at which vegetation responds to ongoing temperature change is still limited. In particular, it is not known whether and to what extent change in the spatial displacement of vegetation productivity isolines during recent decades matches the northward motion of temperature isolines.

The concept of velocity of change[9] offers the opportunity to directly compare the ongoing change in the spatial patterns of temperature and productivity. This concept was first developed for climate impact research to compare the displacement rate of a forcing variable (e.g. temperature) with that of an impacted variable (e.g. the occurrence of a given species) by converting them into the same units[4-9,20] (e.g. km $yr^{-1}$). The velocity of change in a geospatial variable is the ratio of its temporal change to its local geographical gradient[5-7,21,22]. Imagine, for

instance, that the mean spring temperature has increased by 0.3ºC over 30 years. At the same location, a 1°C temperature spatial gradient is observed across a 100 km distance with a south-to-north decrease in temperature. The velocity of spring temperature change is then 1 km $yr^{-1}$ for this example (temporal trend of 0.3ºC over 30 years, divided by the spatial gradient of 1ºC over 100 km).

In a similar manner, within the boundaries of a biome, we can calculate the velocity of change in vegetation productivity (also in km $yr^{-1}$). For each local cell, plant productivity responds to the changes in ambient environment condition, whether the responses are through changes in phenology or physiology of plant individuals (in-situ), or changes in community composition (e.g. shrub expansion). Such changes in productivity for each of the multiple pixels over a region eventually appear as the movement of productivity isolines at regional scale (Supplementary Figure 1a). In this case, the velocity of productivity change indicates a displacement in the isolines of this variable due to changes in productivity in response to climate change for multiple pixels over a certain region (Supplementary Figure 1b). In another word, the concept of velocity here quantifies how the spatial pattern of vegetation productivity changes in response to environmental changes during the study period, with different speeds and directions for each pixel. For a certain location with a south-to-north decrease in vegetation productivity, a northward velocity of vegetation productivity of 1 km $yr^{-1}$ over the past 30 years would indicate that the current productivity of a certain ecosystem has increased from its value 30 years ago to a higher value today equaling to the past productivity of another ecosystem which is 30 km (1 km $yr^{-1}$×30 years) south of the target one. The comparison between the velocities of change in vegetation productivity and temperature then makes it possible to identify if the motion of productivity isolines is in the same directions of that of temperature isolines, or / and if the displacement of productivity isolines is faster/slower than that of

94 temperature isolines. Then we can address the question of whether and to what extent changes
95 in the spatial pattern of vegetation productivity during recent decades have matched the
96 displacement of temperature isolines (Supplementary Information S1.1).
97
98 In this study, we mapped for the first time the vector (both velocity and direction) of change in
99 vegetation productivity calculated using satellite-derived long-term Normalized Difference
100 Vegetation Index (NDVI). The NDVI dataset covers the period of 1982-2011 and was analyzed
101 for velocity in the region north of 50°N, where vegetation productivity responds mainly to
102 temperature changes[23,24]. Productivity velocities were then compared to those of temperature
103 change (see Methods). To minimize the covariate effects of other environmental variables, our
104 analyses focused only on the overlap of natural ecosystems (defined following the International
105 Geosphere-Biosphere Program; see Methods; Supplementary Figure 2) and ecosystems where
106 productivity is temporally positively ($p$<0.1) correlated with temperature during the study
107 period (see Methods; Supplementary Figure 3). This study area represents about 76% of the
108 vegetated area (annual mean NDVI>0.1) over the northern high latitudes.
109
110 We first calculated the distribution of the velocities and their directions for the sum of the April
111 to October growing season (GS) NDVI ($NDVI_{GS}$) and GS mean temperature ($T_{GS}$) over the last
112 30 years (see Methods). The average $NDVI_{GS}$ velocity is 2.8±1.1 km $yr^{-1}$ over the study area.
113 Large $NDVI_{GS}$ velocities (>10 km $yr^{-1}$) are found in eastern Europe, northeastern and western
114 Siberia, and low values (<1 km $yr^{-1}$) in central and eastern Canada as well as western Siberia
115 (Fig. 1a). In 89% of the study area, the directions of $NDVI_{GS}$ vectors are from regions with
116 higher $NDVI_{GS}$ values to those with lower values, with the majority of the study area (55%)
117 showing a northward movement (Fig. 1c). On average, $T_{GS}$ velocity over the study area (5.4±1.0
118 km $yr^{-1}$) is nearly twice the $NDVI_{GS}$ velocity. The largest $T_{GS}$ velocities (>10 km $yr^{-1}$) are

observed in northern central and eastern Siberia, parts of Europe, as well as eastern and northeastern Canada, whereas low values (<1 km $yr^{-1}$) are found only in southwestern Canada (Fig. 1b). Northward $T_{GS}$ vectors are observed in 71% of the study area (Fig. 1d).

Comparing the vectors of $NDVI_{GS}$ and $T_{GS}$ (see Methods), we found that, across the study area, 91% of the study area show a positive ratio between the velocities of projected $NDVI_{GS}$ vectors and the velocities of $T_{GS}$ vectors ($V_N$:$V_T$ ratio) (blue color in Fig. 1e). This suggests that in these regions, vegetation productivity has tracked the direction of temperature change during the study period. Among these regions, about 98% of the area show positive trends in both $NDVI_{GS}$ and $T_{GS}$, that is, vegetation productivity has increased where temperature warmed. Only a few regions in western Canada with positive $V_N$:$V_T$ ratio show decreasing $NDVI_{GS}$ as a result of decreasing $T_{GS}$ during the study period (Supplementary Figure 4). Larger $NDVI_{GS}$ velocities (projected along the $T_{GS}$ velocities) than $T_{GS}$ velocities occur in 20% of the whole study area, mainly in eastern Europe, northeastern and southern Siberia, as well as parts of western Canada (Fig. 1e). In about half of the study area, the $V_N$:$V_T$ ratio is lower than 0.5, in particular northern Europe, central Siberia, and northeastern Canada. Similar results are also obtained when using different climate forcing datasets, when choosing different GS definitions (May to September or April to September), or when $NDVI_{GS}$ velocities were compared with those of mean annual temperature (Supplementary Figure 5; see also Methods).

Overall, the largest $V_N$:$V_T$ ratios are found in relatively warmer regions (Supplementary Figure 6; R=0.89, $p$<0.01). Several possible reasons may explain this phenomenon. First, the ubiquitous $CO_2$ fertilization effect, which can amplify the warming-induced positive trend of productivity[3], is expected to be relatively stronger at higher temperature[25,26]. Second, larger $V_N$:$V_T$ ratios in warmer regions may arise from larger nitrogen availability, either from

144 increased soil nitrogen mineralization or from additional nitrogen deposited to ecosystems in
145 most of the warmer temperate regions of the northern hemisphere[27,28]. In addition, the lower
146 $V_N$:$V_T$ ratios found in colder climates may be associated with background limitations induced
147 from the presence of permafrost (Supplementary Figure 7). Permafrost constrains the
148 development of roots, and slows down the decompositions of soil organic matter limiting
149 mineral nitrogen and phosphorus availability for plants[29].
150
151 In general, vegetation productivity north of 50°N is mainly limited by two factors: growing
152 season length and growing season maximum photosynthetic capacity[24,30]. Growing season
153 length is determined by the start of the growing season (SOS) and the end of the growing season
154 (EOS), which are closely associated with temperature[23], while peak growing season
155 photosynthetic capacity can be partly reflected by the maximum NDVI in the growing season
156 (MOS), which is jointly controlled by nutrient availability and temperature for the study area[31].
157 Hence, we analyzed separately the vectors of NDVI-derived SOS, EOS, and MOS, respectively
158 (see Methods), as shown in Fig. 2.
159
160 The average velocity of change in the SOS date during 1982-2011 is 3.6±1.0 km $yr^{-1}$ over the
161 study area. Pronounced differences in both velocity and direction of SOS vectors can be seen
162 between Eurasia and North America in Fig. 2a and 2d, respectively. The majority of Eurasia
163 (74%) show northward SOS vectors (related to the advance in spring phenology), while only
164 half of North America display northward SOS vectors (Fig. 2d). In Eurasia, the velocity of SOS
165 vectors exceeds 5 km $yr^{-1}$ in 61% of the whole area, whereas in most of North America (73%
166 of the continent area north of 50°N), it is lower than 5 km $yr^{-1}$ (Fig. 2a). The largest SOS
167 velocities (>20 km $yr^{-1}$) are observed in northeastern Siberia. This area also experiences the
168 largest (>10 km $yr^{-1}$) velocities of springtime (March to May, MAM) temperature increase

(Supplementary Figure 8a). In addition, we found that about one third of the study area shows larger velocities of SOS vectors (projected along the spatial gradient of spring temperature) than those of spring temperature vectors themselves (Fig. 2g). These regions include central Europe, central and southern Siberia, as well as parts of eastern and northwestern Canada. By contrast, in western and northeastern Siberia, the velocities of projected SOS vectors are smaller than those of the vectors of springtime temperature (ratio<0.5). Moreover, for 17% of the study area, mainly in Canada, the SOS vectors do not parallel the direction of temperature vectors (red color in Fig. 2g). In eastern and central Canada, a delayed SOS date occurs with warming, whereas in western Canada, an earlier SOS date occurs despite the cooling trend of spring temperature (Supplementary Figure 9a and 10a). Such mismatches may be attributed to changes in the relationship between heat requirement and chilling accumulation (the duration and/or sum of cold temperature during dormancy) due to changes in the late-winter and spring temperature[32-34].

It has been reported that the temperature sensitivity of EOS is lower than that of SOS, because changes in EOS are co-limited by other factors than temperature[31,35,36] (e.g., photoperiod and soil moisture). At first sight, our analysis of EOS velocities suggests the opposite result: the average EOS velocity across the study area (6.0±1.1 km $yr^{-1}$) is nearly twice the SOS velocity (3.6±1.0 km $yr^{-1}$) during 1982-2011. Nearly 60% of the study area display EOS velocities larger than 5 km $yr^{-1}$ (Fig. 2b). However, change in mean temperature from August to October displays a much higher average velocity (7.1±1.0 km $yr^{-1}$) than that in spring temperature (3.7±1.0 km $yr^{-1}$), rendering their average warming dependency more similar. In any case, the co-regulation of EOS by other factors likely explains the much more heterogeneous pattern of the directions of EOS vectors (Fig. 2e) than that of SOS vectors (Fig. 2d). Comparing EOS and August to October mean temperature vectors, we found that regions where the velocities of projected EOS

vectors exceed those of the original temperature vectors are located mainly in southern Siberia as well as in northeastern and southwestern Canada, accounting for 36% of the study area (Fig. 2h). By contrast, northeastern Siberia and eastern Canada experience very strong warming during August-October (Supplementary Figure 10b), but the EOS vectors in these regions show generally lower velocity than in southeastern Siberia (Fig. 2b), resulting in a smaller ratio (<0.5) of EOS to autumn temperature change velocities (Fig. 2h). In parts of central Siberia and western Canada, we even observe an advanced EOS date with warming temperature (red color in Fig. 2h). This mismatch between the vectors of EOS and temperature change may be partly explained by the decreased solar radiation in these regions[36]. Since it has been suggested that increases in solar radiation suppress the accumulation of abscisic acid and subsequently slow the speed of leaf senescence[37], the decline in solar radiation may have resulted in advanced EOS dates despite the warming temperature.

On average, the northern high latitudes exhibit an average MOS velocity of 3.1±1.0 km $yr^{-1}$ over the past three decades, which is lower than that of summer (June to July) temperature (4.2±1.1 km $yr^{-1}$). MOS velocities larger than 10 km $yr^{-1}$ are found in eastern Europe, northeastern Siberia and northeastern Canada, while values lower than 1 km $yr^{-1}$ mainly appear in the southern part of central Siberia, as well as in central and eastern Canada (Fig. 2c). Comparison between the velocity of MOS vectors (projected along the spatial gradient of summer temperature) and that of summer temperature vectors (Fig. 2i) show that larger MOS than temperature change velocities mainly occur in eastern Europe, northeastern Siberia, as well as in western and northeastern Canada, accounting for one third of the area where changes in MOS have tracked the direction of the temperature change (blue color in Fig. 2i). In northwestern Europe and southern Siberia, however, MOS velocities are generally less than half of summer temperature velocities. Since northern ecosystems are strongly temperature-

219 limited[2], the slower velocities of projected MOS vectors compared to summer temperature
220 velocities may be partly attributed to the fact that photosynthesis at the peak of the growing
221 season is constrained because the low-temperature-induced nutrient limitations do not allow the
222 development of dense canopies[38]. Interestingly, we found larger MOS velocities in shrub and
223 tundra ecosystems (3.4±1.0 km $yr^{-1}$ on average) (vegetation types from the International
224 Geosphere-Biosphere Program; Supplementary Figure 2) than in other vegetation types. Also
225 the ratio of velocities of projected MOS vectors to summer temperature velocities is highest in
226 shrub and tundra (Supplementary Table 1). Warming-induced tall shrub and tree expansion[39]
227 may be responsible for the larger MOS velocities in shrub and tundra than in other terrestrial
228 ecosystems.
229
230 Land surface models are used to project future responses of ecosystems to climate change and
231 to analyze the contribution of different driving factors[40]. We therefore examined the vectors of
232 change in vegetation productivity using simulated net primary productivity (NPP) from five
233 process-based land surface models (CLM4.5, LPJG, OCN, ORCHIDEE, and VEGAS; see
234 Methods and Supplementary Table 2). Our results show that the ensemble model-mean of
235 change in annual NPP displays an average velocity of 4.0±1.3 km $yr^{-1}$ (±standard deviation
236 across models). The highest NPP velocity values (>10 km $yr^{-1}$) are found in southern and
237 northeastern Siberia (Supplementary Figure 11a). We next compared the velocities of simulated
238 NPP with those of $NDVI_{GS}$ after projecting both NPP and $NDVI_{GS}$ vectors along the spatial
239 gradient of $T_{GS}$ (see Methods). The results show that, on average, about 60% of the study area
240 (ranging from 47% to 70% across different models) show higher velocities of simulated NPP
241 than of $NDVI_{GS}$. Further, we examined the NPP velocities using a satellite-derived terrestrial
242 NPP product ($GIMMS_{3g}$ NPP; see Methods), which display spatial patterns consistent with
243 those of the $NDVI_{GS}$ vectors (for both velocity and direction), albeit with generally lower

velocity across the study area (Supplementary Figure 12). Compared with the $GIMMS_{3g}$ NPP, the model-simulated NPP produces larger velocity in about 71% (ranging from 61% to 81%) of the study area. This mismatch regarding the increase in productivity under warming between model- and satellite-based estimates may partly be explained by the limited availability of nitrogen in these regions[41], which is suggested to prevent changes in vegetation productivity from adequately tracking the warming trend, but are not accounted for in some of the models[42]. Interestingly, we found that the two models with nitrogen limitations and nitrogen deposition taken into consideration (CLM4.5 and OCN) both produce lower NPP velocities (1.7±1.0 km $yr^{-1}$ and 2.0±1.1 km $yr^{-1}$ for CLM4.5 and OCN, respectively) than those without a coupled nitrogen cycle (3.5±1.0 km $yr^{-1}$, 2.9±1.1 km $yr^{-1}$ and 4.7±1.2 km $yr^{-1}$ for LPJG, ORCHIDEE and VEGAS, respectively) (Supplementary Table 3). Similar results are also observed for gross primary productivity (GPP; Supplementary Table 3 and Figure 13).

In summary, in this study we applied the concept of velocity to remotely sensed NDVI fields and compared the NDVI velocity to that of temperature in northern (predominantly temperature limited) ecosystems north of 50°N. The average velocity of change in $NDVI_{GS}$ (2.8±1.1 km $yr^{-1}$) over the study area is only about half of that in $T_{GS}$ (5.4±1.0 km $yr^{-1}$). A mismatch between the $NDVI_{GS}$ and $T_{GS}$ velocities suggests that the ratio of sensitivities of productivity to temperature across space and in time is not equal to one (Supplementary Information S2.1). Our analyses thus combined time and space and to some extent challenged the space-for-time substitution hypothesis[43] as applied in several studies using spatial gradients to back-cast temporal changes. Moreover, such a mismatch between productivity and temperature velocities suggests a disequilibrium in the plasticity of vegetation productivity changes to tail off with the spatial spread of warming. This may due to the prevalence of background spatial limitations by other factors limiting vegetation productivity such as soil moisture and nutrients[18], which also

correspond to vegetation acclimation to the ongoing warming[17], as well as the transient limitations in the rate of adjustment of plant response to the warming rate in different seasons. In addition, differences in the magnitudes of the SOS, EOS and MOS velocities suggest that the seasonal profile of vegetation growth has strongly re-shaped over time and that limitations may be expected in spring phenology not being able to track temperature moving northward (e.g. for photoperiod limitations, chilling requirements reasons[32-34]).

## Methods

**Data.** The monthly air temperature data set used in this study is the CRU TS 3.22 climate data set obtained from Climatic Research Unit (CRU) for the period January 1982 to December 2011 (http://www.cru.uea.ac.uk/cru/data/hrg/). We also used WATCH Forcing Data Methodology to ERA-Interim data with temporal resolution of 3 hour (WFDEI)[44]. The third generation Global Inventory Monitoring and Modeling System Normalized Difference Vegetation Index (GIMMS $NDVI_{3g}$) data set from the Advanced Very High Resolution Radiometer (AVHRR) sensors was downloaded from http://ecocast.arc.nasa.gov/data/pub/gimms/3g.v0/. The data set has 15-day temporal frequency from July 1981 to December 2011 with a spatial resolution of 8 km[45]. Only positive NDVI values from January 1982 to December 2011 were used in this study. We also used a 16-day NDVI datasets retrieved using observations from Terra Moderate Resolution Imaging Spectroradiometer (MODIS) (MODIS NDVI) from February 2000 to July 2012 with spatial resolutions of 1 km[46] to test the robustness of the analyses conducted with GIMMS $NDVI_{3g}$ data. A 30-year (1982-2011) satellite-derived terrestrial net primary productivity (NPP) data set presented in a recent study[47], which was calculated using GIMMS leaf area index (LAI) and fraction of photosynthetically active radiation absorbed by the vegetation (FPAR) based on MODIS NPP algorithm[47], was also used. Note that the spatial structures of the error in the surfaces of NDVI and temperature may be different due to different approaches to obtain

gridded datasets. For example, the NDVI differences between neighboring cells obtained from composite AVHRR images may be more contrasted than those of climate data being obtained by interpolation of station data or re-analysis with numerical weather prediction models. To reduce the effect of fine scale spatial structure in the errors on each surface, all the data have been regridded into a common 1°×1° grid. A mask is applied whereby grid cells where annual mean NDVI is less than 0.1 are excluded to remove areas with very low ecosystem productivity. Vegetation types defined following the International Geosphere-Biosphere Program based on a MODIS land cover classification (http://webmap.ornl.gov/wcsdown/wcsdown.jsp?dg_id=10011_1) were used to further remove hardly natural and non-natural vegetation lands.

**Satellite-derived indexes of vegetation productivity.** The maximum NDVI value at each bimonthly time step was used to calculate monthly NDVI in order to minimize the effects of atmospheric water vapor, non-volcanic aerosols and cloud-cover[45]. The growing season (GS) NDVI ($NDVI_{GS}$) was calculated as the sum of monthly NDVI values from April to October. GS defined as May to September and April to September were also used for robustness test. Note that over the northern high latitudes, calculating $NDVI_{GS}$ with a predefined period is to some extent challenging in the boreal regions because of the snow effect. Therefore, we calculated the percentage of the study area with possible snow effects using he quality flag information of GIMMS $NDVI_{3g}$ datasets[45]. To be specific, when regridding the original 8 km (≈1/12 degree) monthly data into a 1°×1° gridded monthly data, a 1°×1° pixel is considered to be affected by snow in this month if less than 70% pixels within a 12×12 pixel window have a flag value of 1 or 2 (good value). For each year, a pixel is then considered to be affected by snow if more than 2 months during the predefined growing season (e.g. April-October) is affected by snow. Finally, we defined regions with snow effects as pixels with more than 9 years showing snow

effects during the study period. The results show that regions affected by snow are mainly located in Alaska, northern Europe and parts of eastern Siberia, accounting for only 12% of the study area (red color in Supplementary Figure 14).

Two phenological indexes were derived from GIMMS $NDVI_{3g}$ data set: the start of growing season (SOS, DOY) and the end of growing season (EOS, DOY). The SOS date was calculated as the averaged SOS date estimated by four different methods: Timesat, Spline, Hants and Polyfit[48-50]. The EOS date was obtained from the averaged EOS estimated by four different methods: Hants, Polyfit, Double Logistic and Piecewise Logistic[36]. For each year during 1982-2011, the maximum NDVI of growing season (MOS) was calculated as the peak NDVI value among monthly NDVI values during the growing season, which was defined based on the month when the SOS and EOS date occurred.

**Model-simulated ecosystem productivity.** We used NPP and gross primary productivity (GPP) outputs from 1982 to 2011 from five process-based land surface models: CLM4.5, LPJG, OCN, ORCHIDEE, and VEGAS (see model list in Supplementary Table 2). All models were run based on the TRENDY inter-comparison protocol during the period 1901-2010 using the same observed climate drivers from CRU-NCEP Version 4 (http://dods.extra.cea.fr/data/p529viov/cruncep/), rising atmospheric $CO_2$ from the combination of ice core records and atmospheric observations, and land use change from the Hyde database (http://dgvm.ceh.ac.uk/node/21). NPP and GPP from all the five models were all resampled into 1°×1° grids.

**The vector of change.** The vector of change in a certain variable takes both velocity and direction into consideration. For each pixel, the velocity was defined as the ratio between the

344 30-year temporal trend and the spatial gradient in 30-year means[4,6,9,51]. Temporal trend was
345 calculated using least squares linear regression for each grid[51]. Spatial gradient was calculated
346 using a 3×3 grid cell neighborhood based on the average maximum technique[9]. Following
347 Loarie *et al.*[9], to convert cell height in latitudinal degrees to km, we used 111.325 km degree$^{-1}$.
348 To convert cell width in longitudinal degrees to km, we calculated $\cos\left(\frac{\pi}{180}y\right)111.325$, in
349 which y is the latitude of the pixel in degrees. We also added a uniformly distributed random
350 noise to each pixel to decrease the incidence of flat spatial gradients that cause infinite velocity
351 values[9]. For temperature, a random noise from -0.05 to 0.05 °C was used; for $NDVI_{GS}$ and the
352 maximum NDVI value during growing season (MOS), a random noise from -0.005 to 0.005
353 was used; for the start / end of the growing season (SOS / EOS), a random noise from -0.05-
354 0.05 DOY was used; for NPP / GPP, a random noise from -0.5-0.5 gC m$^{-1}$ yr$^{-1}$ was used. The
355 direction of each vector was determined from the orientation of the spatial gradient, together
356 with the direction of change in a particular variable[4]. For example, if temperature showed a
357 positive trend during the study period, then the direction of temperature vector is towards areas
358 that used to be cooler. Therefore, assuming a south-to-north decrease in temperature over the
359 study area, then a northward (that is, along the spatial gradient) temperature vector indicates a
360 warming temperature during the study period. Similarly, a northward $NDVI_{GS}$ vector refers to
361 an increase in $NDVI_{GS}$ during the study period. A northward SOS vector is evidence for an
362 earlier trend in SOS date, while for EOS, a northward vector is evidence for a delayed EOS
363 date during the study period. A northward MOS vector is associated with a positive trend of
364 MOS at the local pixel during the study period.
365
366 We compared the velocity of change in $NDVI_{GS}$ derived from GIMMS $NDVI_{3g}$ with the one
367 obtained from MODIS NDVI during 2001-2011. The processing of MODIS NDVI datasets is
368 based on spectral bands that are specifically designed for vegetation monitoring and take state-

of-the-art navigation, atmospheric correction, reduced geometric distortions and improved radiometric sensitivity into consideration[46]. MODIS NDVI is considered to be an improvement over the NDVI product derived from the AVHRR sensors[46,52], but it also has the disadvantage of shorter time span compared to GIMMS $NDVI_{3g}$. Generally, the $NDVI_{GS}$ velocity from MODIS NDVI shows similar spatial pattern to that from GIMMS $NDVI_{3g}$, even though larger values of the former than the latter in parts of central, northern and northeastern Canada (Supplementary Figure 15).

**Analysis.** This study covered regions where vegetation productivity was temporally significantly ($p$<0.1) correlated with temperature from 1982 to 2011. Assuming a linear relationship between vegetation productivity and temperature, the strength (correlation) of the linkage between the two variables was determined by the Pearson correlation coefficient between the time series of $NDVI_{GS}$ and GS mean temperature, i.e., between the time series of the sum of monthly NDVI during April-October and the mean temperature during April-October. To compare the vectors of vegetation productivity and temperature velocities, for each grid cell, we calculated the ratio between the velocity of vegetation productivity ($V_V$) along the spatial gradient of temperature ($V_V$') and the velocity of temperature ($V_T$). Here $V_V$' was computed as the velocity of the vegetation vector after projecting it along the spatial gradient of temperature, which can expressed as $V_{V'} = |V_V| \times \cos(|A_T - A_V|)$, where $A_T$ and $A_V$ is the vector angle (in radians) for metrics of temperature and vegetation productivity, respectively. The sign of the ratio between $V_{V'}$ and $V_T$ was determined from the directions of both vectors. For a given pixel, a positive ratio is observed if the vector of change in vegetation productivity displays the same direction as the vector of temperature change, suggesting that change in the spatial pattern of vegetation productivity was directionally consistent with that of temperature. A negative ratio indicates that the directional change in the spatial patterns of the two variables

were of opposite directions. The $NDVI_{GS}$ vector was compared with the vector of GS mean temperature with different definitions of GS: April to October, May to September, and April to September. Comparisons of vector of $NDVI_{GS}$ and that of mean annual temperature were also presented. Since the timing of vegetation phenology is associated with temperature of the preceding 0-3 months[36,53], here the vector of change in the SOS and EOS date were compared with that of change in mean temperature during March to May and August to October, respectively. The vector of change of MOS was compared with that of change in mean temperature during June to July. Note that since it has been well recognized that increasing spring temperature (i.e. positive trend of temperature) tends to result in an earlier SOS date (i.e. negative trend of SOS date) over most of northern ecosystems during the past three decades[54], regions where the change in vegetation productivity were consistent with warming trend refer to those with a negative trend in SOS date during the study period. The vectors of change in satellite-derived NPP, as well as model-simulated annual NPP and GPP were calculated using the same methods as calculating $NDVI_{GS}$ vectors, and compared with the vector of change in GS (April to October) mean temperature.

## References


1 Elmendorf, S. C. *et al.* Plot-scale evidence of tundra vegetation change and links to recent summer warming. *Nat. Clim. Chang.* **2**, 453-457 (2012).

2 Nemani, R. R. *et al.* Climate-driven increases in global terrestrial net primary production from 1982 to 1999. *Science* **300**,1560-1563 (2003).

3 Zhu, Z. *et al.* Greening of the Earth and its drivers. *Nat Clim Chang* **6**, 791-795 (2016).

4 Ackerly, D. *et al.* The geography of climate change: implications for conservation biogeography. *Divers. Distrib.* **16**, 476-487 (2010).

5 Burrows, M. T. *et al.* The pace of shifting climate in marine and terrestrial ecosystems. *Science* **334**, 652-655 (2011).

6 Burrows, M. T. *et al.* Geographical limits to species-range shifts are suggested by climate velocity. *Nature* **507**, 492-495 (2014).

7 Diffenbaugh, N. S. & Field C. B. Changes in ecologically critical terrestrial climate conditions. *Science* **341**, 486-492 (2013)

8 Dobrowski, S. Z. *et al.* The climate velocity of the contiguous United States during the 20th century. *Glob. Chang Biol.* **19**, 241-251 (2013).

9 Loarie, S. R. *et al.* The velocity of climate change. *Nature* **462**, 1052-1055 (2009).

10 Parry, M. L. *Climate change 2007-impacts, adaptation and vulnerability: Working group II contribution to the fourth assessment report of the IPCC*, Cambridge University Press (2007).

11 Buitenwerf, R., Rose, L. & Higgins, S. I. Three decades of multi-dimensional change in global leaf phenology. *Nat. Clim. Chang.* **5**, 364-368 (2015).

12 Vitasse, Y., Porté, A. J., Kremer, A., Michalet, R. & Delzon, S. Responses of canopy duration to temperature changes in four temperate tree species: relative contributions of spring and autumn leaf phenology. *Oecologia* **161**, 187-198 (2009).

13 Wolkovich, E. M. *et al.* Warming experiments underpredict plant phenological responses to climate change. *Nature* **485**, 494-497 (2012).

14 Wu, Z., Dijkstra, P., Koch, G. W., Peñuelas, J. & Hungate B. A. Responses of terrestrial ecosystems to temperature and precipitation change: a meta-analysis of experimental manipulation. *Glob. Chang Biol.* **17**, 927-942 (2011).

15 Peñuelas, J. & Filella, I. Responses to a warming world. *Science* **294**, 793-795 (2001).

16 Penuelas, J. *et al.* Evidence of current impact of climate change on life: a walk from genes to the biosphere. *Glob. Chang Biol.* **19**, 2303-2338 (2013).

17 Hikosaka, K., Ishikawa, K., Borjigidai, A., Muller, O. & Onoda, Y. Temperature acclimation of photosynthesis: mechanisms involved in the changes in temperature dependence of photosynthetic rate. *J. Exp. Bot.* **57**, 291-302 (2006).

18 Way, D. A. & Oren, R. Differential responses to changes in growth temperature between trees from different functional groups and biomes: a review and synthesis of data. *Tree Physiol.* **30**, 669-688 (2010).

19 Thomas, R. Q., Canham, C. D., Weathers, K. C. & Goodale, C. L. Increased tree carbon storage in response to nitrogen deposition in the US. *Nat. Geosci.* **3**, 13-17 (2010).

20 Sandel, B. *et al.* The influence of Late Quaternary climate-change velocity on species endemism. *Science* **334**, 660-664 (2011).

21 Bi, J., Xu, L., Samanta, A., Zhu, Z. & Myneni, R. Divergent arctic-boreal vegetation changes between North America and Eurasia over the past 30 years. *Remote Sens.* **5**, 2093-2112 (2013).

22 LoPresti, A. *et al.* Rate and velocity of climate change caused by cumulative carbon emissions. *Environ. Res. Lett.* **10**, 095001 (2015).

23 Lucht, W. *et al.* Climatic control of the high-latitude vegetation greening trend and Pinatubo effect. *Science* **296**, 1687-1689 (2002).

24 Myneni, R. B., Keeling, C. D., Tucker, C. J., Asrar, G. & Nemani, R. R. Increased plant growth in the northern high latitudes from 1981 to 1991. *Nature* **386**, 698-702 (1997).

462 25 Hickler, T. *et al.* $CO_2$ fertilization in temperate FACE experiments not representative of
463 boreal and tropical forests. *Glob. Chang Biol.* **14**, 1531-1542 (2008).
464 26 Schimel, D., Stephens, B. B. & Fisher, J. B. Effect of increasing $CO_2$ on the terrestrial
465 carbon cycle. Proc. Natl. Acad. Sci. U.S.A. **112**, 436-441 (2015).
466 27 Granath, G. *et al.* Photosynthetic performance in Sphagnum transplanted along a
467 latitudinal nitrogen deposition gradient. *Oecologia* **159**, 705-715 (2009).
468 28 Livingston, N., Guy, R., Sun, Z. & Ethier, G. The effects of nitrogen stress on the stable
469 carbon isotope composition, productivity and water use efficiency of white spruce
470 (*Picea glauca* (Moench) Voss) seedlings. *Plant Cell Environ.* **22**, 281-289 (1999).
471 29 Kimball, J. S. *et al.* Recent climate-driven increases in vegetation productivity for the
472 western arctic: evidence of an acceleration of the northern terrestrial carbon cycle. *Earth*
473 *Interact.* **11**, 1-30 (2007).
474 30 Xia, J. *et al.* Joint control of terrestrial gross primary productivity by plant phenology
475 and physiology. *Proc. Natl. Acad. Sci. U.S.A.* **112**, 2788-2793 (2015).
476 31 Forkel, M. *et al.* Codominant water control on global interannual variability and trends
477 in land surface phenology and greenness. *Glob. Chang Biol.* **21**, 3414-3435 (2015).
478 32 Fu, Y. H. *et al.* Declining global warming effects on the phenology of spring leaf
479 unfolding. *Nature* **526**, 104-107 (2015).
480 33 Laube, J. *et al.* Chilling outweighs photoperiod in preventing precocious spring
481 development. *Glob. Chang Biol.* **20**, 170-182 (2014).
482 34 Zhang, X., Tarpley, D. & Sullivan, J. T. Diverse responses of vegetation phenology to a
483 warming climate. *Geophys. Res. Lett.* **34**, L19405 (2007).

35 Barichivich, J. *et al.* Large-scale variations in the vegetation growing season and annual cycle of atmospheric $CO_2$ at high northern latitudes from 1950 to 2011. *Glob. Chang Biol.* **19**, 3167-3183 (2013).

36 Liu, Q. *et al.* Temperature, precipitation, and insolation effects on autumn vegetation phenology in temperate China. *Glob. Chang Biol.* **22**, 644-655 (2016).

37 Gepstein, S. & Thimann, K. V. Changes in the abscisic acid content of oat leaves during senescence. *Proc. Natl. Acad. Sci. U.S.A.* **77**, 2050-2053 (1980).

38 Melillo, J. M. *et al.* Soil warming, carbon-nitrogen interactions, and forest carbon budgets. *Proc. Natl. Acad. Sci. U.S.A.* **108**, 9508-9512 (2011).

39 Frost, G. V. & Epstein, H. E. Tall shrub and tree expansion in Siberian tundra ecotones since the 1960s. *Glob. Chang Biol.* **20**, 1264-1277 (2014).

40 Sitch, S. *et al.* Evaluation of the terrestrial carbon cycle, future plant geography and climate-carbon cycle feedbacks using five Dynamic Global Vegetation Models (DGVMs). *Glob. Chang Biol.* **14**, 2015-2039 (2008).

41 Fisher, J. B., Badgley, G. & Blyth, E. Global nutrient limitation in terrestrial vegetation. *Glob. Biogeochem. Cycles* **26**, GB1014 (2012).

42 Likens G. *Long-term Studies in Ecology* (Springer, 1989).

43 Smith, N. G. & Dukes, J. S. Plant respiration and photosynthesis in global-scale models: incorporating acclimation to temperature and $CO_2$. *Glob. Chang Biol.* **19**, 45-63 (2013).

44 Weedon, G. P. *et al.* The WFDEI meteorological forcing data set: WATCH Forcing Data methodology applied to ERA-Interim reanalysis data. *Water. Resour. Res.* **50**, 7505-7514 (2014).

506 45 Pinzon, J. E. & Tucker, C. J. A non-stationary 1981–2012 AVHRR NDVI3g time series.
507 *Remote Sens.* **6**, 6929-6960 (2014).
508 46 Huete, A. *et al.* Overview of the radiometric and biophysical performance of the MODIS
509 vegetation indices. *Remote Sens. Environ.* **83**, 195-213 (2002).
510 47 Smith, W. K. *et al.* Large divergence of satellite and Earth system model estimates of
511 global terrestrial $CO_2$ fertilization. *Nat. Clim. Chang.* **6**, 306-310 (2016).
512 48 Cong, N. *et al.* Changes in satellite-derived spring vegetation green-up date and its
513 linkage to climate in China from 1982 to 2010: a multimethod analysis. *Glob. Chang*
514 *Biol.* **19**, 881-891 (2013).
515 49 Piao, S., Fang, J., Zhou, L., Ciais, P. & Zhu, B. Variations in satellite-derived phenology
516 in China's temperate vegetation. *Glob. Chang Biol.* **12**, 672-685 (2006).
517 50 White, M. A. *et al.* Intercomparison, interpretation, and assessment of spring phenology
518 in North America estimated from remote sensing for 1982-2006. *Glob. Chang Biol.* **15**,
519 2335-2359 (2009).
520 51 Zheng, B., Chenu, K. & Chapman, S. C. Velocity of temperature and flowering time in
521 wheat-assisting breeders to keep pace with climate change. *Glob. Chang Biol.* **22**, 921-
522 933 (2016).
523 52 Fensholt, R. & Proud, S. R. Evaluation of earth observation based global long term
524 vegetation trends-Comparing GIMMS and MODIS global NDVI time series. *Remote*
525 *Sens. Environ.* **119**, 131-147 (2012).
526 53 Piao, S. *et al.* Leaf onset in the northern hemisphere triggered by daytime temperature.
527 *Nat. Commun.* **6**, 6911 (2015).

528 54 Jeong, S., Ho, C. H., Gim, H. J. & Brown, M. E. Phenology shifts at start vs. end of
529 growing season in temperate vegetation over the Northern Hemisphere for the period
530 1982–2008. *Glob. Chang Biol.* **17**, 2385-2399 (2011).

531

532 **Acknowledgements**

533 This study was supported by National Natural Science Foundation of China (41530528), and
534 the 111 Project (B14001). IJ, PC, and JP were supported by the European Research Council
535 Synergy grant SyG-2013-610028 IMBALANCE-P

536

537 **Author contributions**

538 S.L.P. designed research; M.T.H. performed analysis; and all authors contributed to the
539 interpretation of the results and the writing of the paper.

540

541 **Author Information**

542 Reprints and permissions information is available at www.nature.com/reprints. The authors
543 have no competing financial interests. Correspondence and requests for materials should be
544 addressed to S.L.P. (slpiao@pku.edu.cn)

545

546

## Figure Legends

**Figure 1 | The velocity of vegetation productivity ($NDVI_{GS}$) and temperature ($T_{GS}$) from 1982 to 2011 over northern high latitudes (north of 50°N).** **a**, The spatial pattern of the velocity of the vector of change in $NDVI_{GS}$. **b**, The spatial pattern of the velocity of the vector of change in $T_{GS}$. **c**, The spatial pattern of the direction of the vector of change in $NDVI_{GS}$. **d**, The spatial pattern of the direction of the vector of change in $T_{GS}$. **e**, The comparison between velocity of $NDVI_{GS}$ vector after projecting along the spatial gradient of $T_{GS}$ and the velocity of $T_{GS}$ vector (see Methods). The growing season is defined as from April to October. The velocity was calculated as the ratio between the 30-year temporal trend and the spatial gradient in 30-year means (see Methods). The velocities shown in panel **a** and **b** are original velocities without projecting the $NDVI_{GS}$ vectors along the temperature gradient. For panel **c** and **d**, 'N', 'NE', 'E', 'ES', 'S', 'SW', 'W' and 'NW' in the legend refer to 'North-ward', 'Northeast-ward', 'East-ward', 'Southeast-ward', 'South-ward', 'Southwest-ward', 'West-ward', and 'Northwest-ward', respectively. For panel **e**, the ratio between the velocity of $NDVI_{GS}$ along the spatial gradient of $T_{GS}$ and the velocity of $T_{GS}$ was calculated after projecting $NDVI_{GS}$ vector along the spatial gradient of $T_{GS}$ for each pixel (see Methods). A blue color (positive ratio) suggests that change in the spatial pattern of $NDVI_{GS}$ was directionally consistent with the direction of change in the spatial pattern of $T_{GS}$, while a red color (negative ratio) indicates that the former was inconsistent with the direction of the latter. Note that only gridded pixels covered by natural vegetation (defined following the International Geosphere-Biosphere Program based on a MODIS land cover classification; Supplementary Figure 2) with annual mean NDVI value larger than 0.1 are shown here.

**Figure 2 | The velocity (a-c) and direction (d-f) of the vector of change in vegetation phenology and physiology over the northern high latitudes (north of 50 °N) from 1982 to**

572 **2011 and comparison with the velocity of corresponding temperature metrics (g-i).**
573 Vegetation phenology is characterized by the start of the growing season (SOS) and end of the
574 growing season (EOS); vegetation physiology is characterized by the maximum NDVI of
575 growing season (MOS). For each pixel, the velocity for a certain variable was calculated as the
576 ratio between the 30-year temporal trend and the spatial gradient in 30-year means for each
577 index (see Methods). The velocities shown in panel **a**-**c** are original velocities without
578 projecting the vegetation vectors along the temperature gradient. 'N', 'NE', 'E', 'ES', 'S', 'SW',
579 'W' and 'NW' in the legend for panel **d**-**f** refer to 'North-ward', 'Northeast-ward', 'East-ward',
580 'Southeast-ward', 'South-ward', 'Southwest-ward', 'West-ward', and 'Northwest-ward',
581 respectively. For panel **g**-**i**, the ratio between the velocity of SOS/EOS/MOS along the spatial
582 gradient of temperature and the velocity of temperature change was calculated after projecting
583 the vectors of change in SOS/EOS/MOS along the spatial gradient of corresponding
584 temperature metric for each pixel (see Methods). A blue color (positive ratio) suggests that
585 change in the spatial pattern of SOS/EOS/MOS was directionally consistent with the direction
586 of change in the spatial pattern of corresponding temperature metric, while a red color (negative
587 ratio) indicates that the former was inconsistent with the direction of the latter. Pie chart of
588 ratios shown in the spatial patterns is shown in the inset at bottom-left of panel **g**-**i**. Note that
589 only gridded pixels covered by natural vegetation (defined following the International
590 Geosphere-Biosphere Program based on a MODIS land cover classification; Supplementary
591 Figure 2) with annual mean NDVI value larger than 0.1 are shown here.
592

593 **Figure 1**

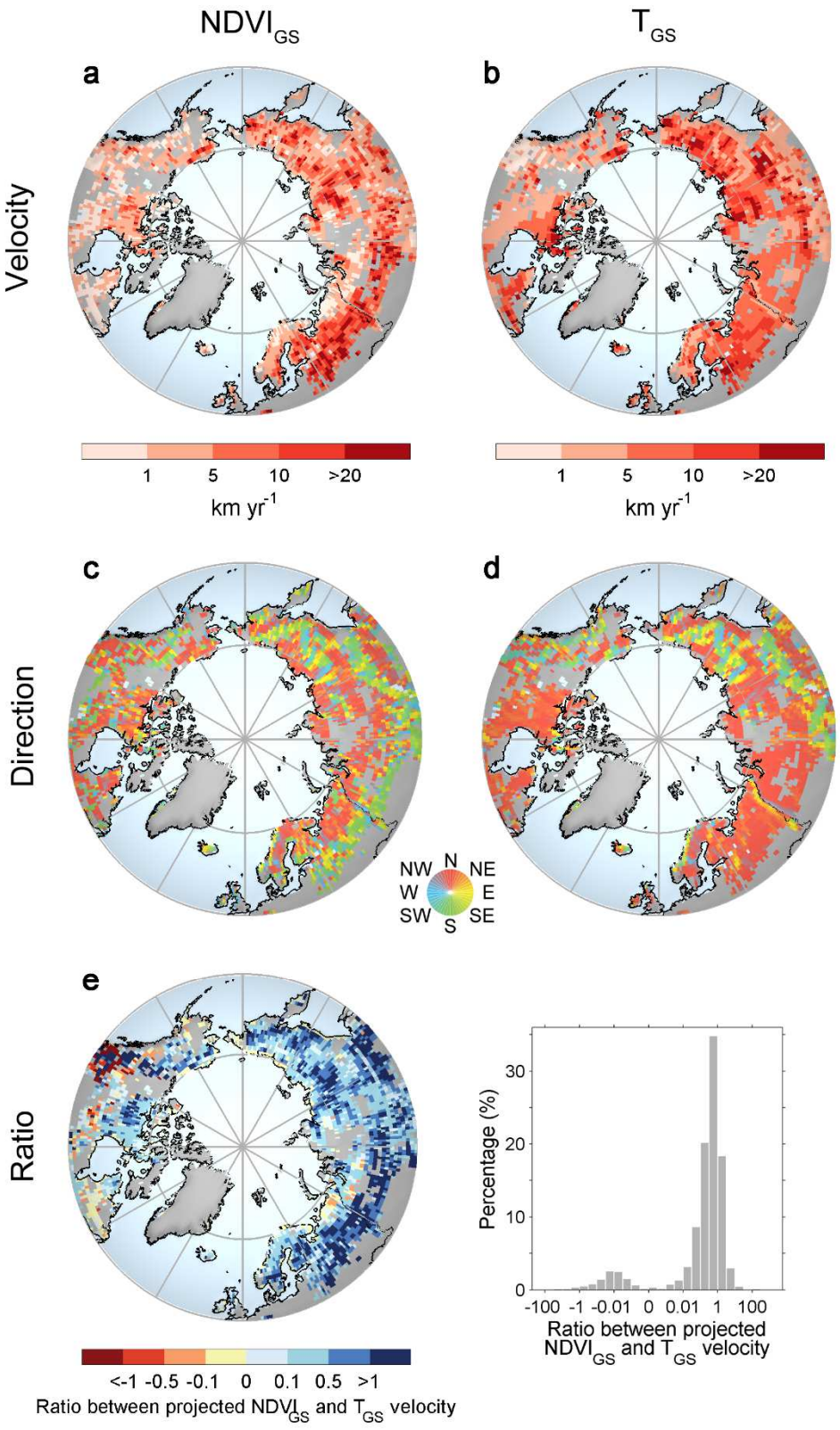


594

595

596 **Figure 2**

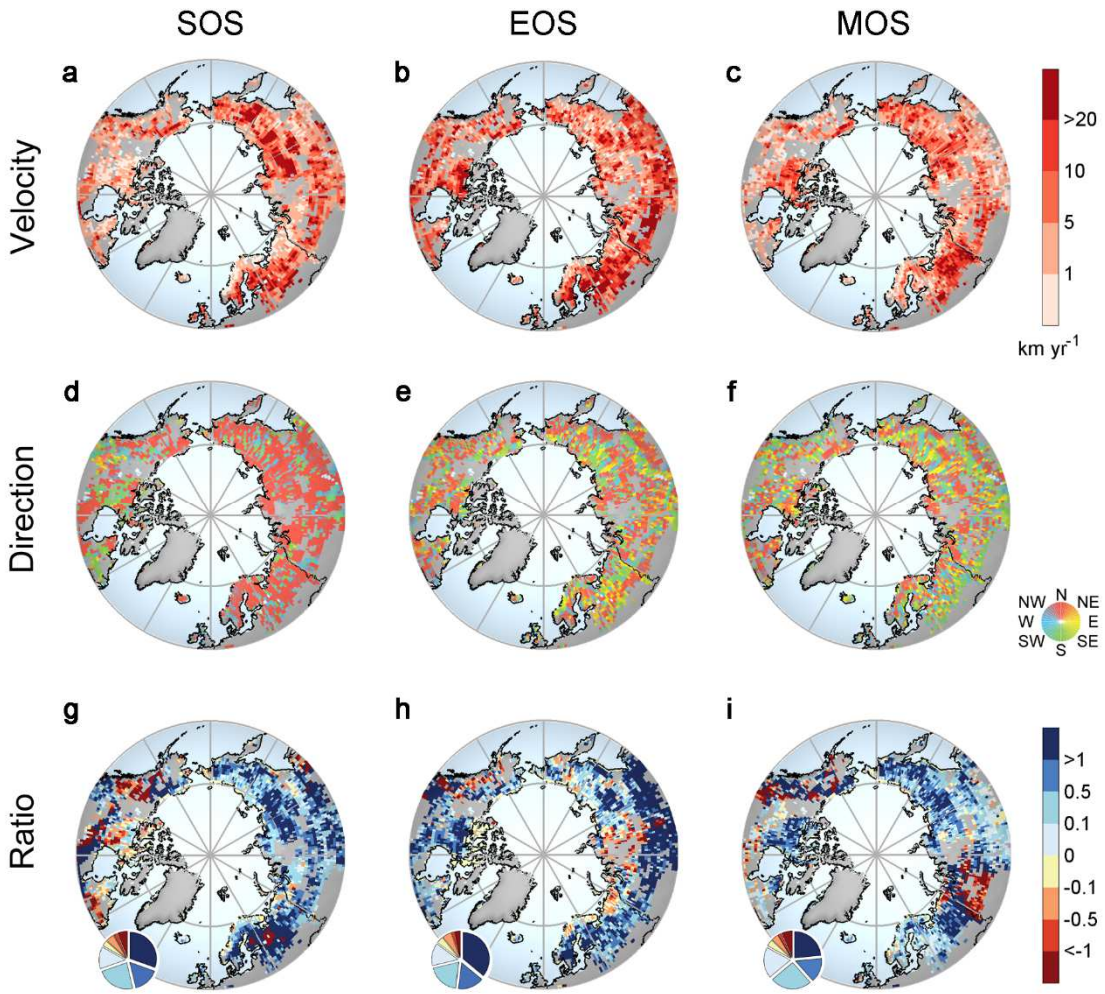


597

598